Enhanced Electromechanical Modeling of Asymmetrical Dual Three-Phase IPMSM Drives

Hisham Eldeeb*, Mohamed Abdelrahem†, Christoph Hackl‡, Ayman Samy Abdel-Khalik§
*Munich School of Engineering, Technical University of Munich (TUM), Munich, Germany. E-mail: hisham.eldeeb@tum.de.
†Institute of Electrical Drive Systems and Power Electronics, TUM, Munich, Germany.
‡Department of Electrical Engineering and Information Technology, Munich University of Applied Sciences, Munich, Germany.
§Electrical Engineering Department, Faculty of Engineering, Alexandria University, Alexandria, Egypt.

***Abstract*—Throughout literature, a clear concern for achieving high performance stator current control of asymmetrical dual three-phase IPMSM drives as well as fault tolerant strategies were demonstrated. However, limited attention was given on how to effectively compute, simulate and compare the expected (i.e. simulated) and the practically applied electromechanical torque. This requires an accurate electromechanical model with precise electromechanical torque estimation. This paper presents a high fidelity *direct-quadrature* (dq) model capable of describing the generated electromechanical torque. The presented method is based on obtaining the non-linear flux linkage maps as well as describing the harmonic models, which contribute to the average and ripple torque, respectively. The flux linkage maps contribute in the tuning of the stator current controllers and electromechanical torque computation, which is compared to the computed torque from the manufacturer parameters and literature. The proposed model does not require previous knowledge concerning geometric and machine design data. The results coincide to a high extent with the experimental validations on a 2.5 kW asymmetrical dual three-phase IPMSM prototype.**

***Index Terms*—Current control, Dual three-phase, IPMSM, modeling.**

NOMENCLATURE

$\mathbb{R}, \mathbb{N}$ are the set of real and natural numbers. $x \in \mathbb{R}$ is a real scalar, while $\boldsymbol{x} \in \mathbb{R}^n$ (bold) is a real valued vector with $n \in \mathbb{N}$. $\boldsymbol{x}^\top$ is the transpose of $\boldsymbol{x}$. $\boldsymbol{X} \in \mathbb{R}^{n \times m}$ (capital bold) is a real valued matrix with $n \in \mathbb{N}$ rows and $m \in \mathbb{N}$ columns. $\boldsymbol{I}_n \in \mathbb{R}^{n \times n} := \mathrm{diag}(1, \ldots, 1)$: identity matrix. $\boldsymbol{O}_n \in \mathbb{R}^{n \times n} := \mathrm{diag}(0, \ldots, 0)$: zero square matrix. The determinant of a square matrix $\boldsymbol{Q}$ is det($\boldsymbol{Q}$). $\boldsymbol{x}_{\mathrm{s}}^{a_1 \to c_2} \in \mathbb{R}^6$ is the stator space vector expressed in the ($\mathrm{a_1b_1c_1\text{-}a_2b_2c_2}$) reference frame and may represent voltage $\boldsymbol{u}$ (V), flux linkage $\boldsymbol{\psi}$ (Wb) or current $\boldsymbol{i}$ (A), i.e. $\boldsymbol{x} \in \{\boldsymbol{u}, \boldsymbol{\psi}, \boldsymbol{i}\}$. The subscript 's' denotes stator quantities. The electromechanical and load torques ($\mathrm{N \cdot m}$), the electrical angular speed (rad/s), electrical angular position (rad) with respect to the reference flux axis of phase a_1, and inertia ($\mathrm{kg{\cdot}m^2}$) are m_{e}, m_{load}, ω_{e}, ϕ_{e}, and Θ, respectively. The viscous friction coefficient is ν ($\mathrm{N \cdot m \cdot s}$), while the coulomb friction is m_{c} (N·m). The electrical resistance (Ω) and inductances (H) are indicated by R and L, respectively. Sampling / switching frequencies is given by f_{sw} (kHz).

I. INTRODUCTION

The rapid development of power electronic devices and real-time embedded systems promoted significantly the adoption of multiphase (i.e. more than three-phases) drives, which are employed when a high level of fault-tolerance and reliability are of interest [1]. Within the last decade, a noticeable amount of literature has been dedicated to dual three-phase (DTM) drives; since dual three-phase machines can be easily realized through rewinding of the existing three-phase stator windings [2]. Such rewinding permits varying the space-orientation of the two three-phase sets with respect to each other. Most popular space angles are *zero*, also known as dual-windings, $\pi/3$ rad symmetrical dual three-phase windings, and $\pi/6$ rad known as asymmetrical dual three phase (ADT) windings [3]. The asymmetrical type has better fundamental flux content over the symmetrical type, but slightly lower fault-tolerance capability [3], [4]. However, this paper deals with the asymmetrical type. Asymmetrical dual three-phase IPMSMs (ADT-IPMSMs) are known for their high efficiency and improved power/weight ratio, when compared to ADT induction machines (ADT-IMs), making ADT-IPMSMs potential candidates for instance for currently emerging technologies as electric vehicles [5].

Zhao et. al. in [6] initiated the principle of harmonics distribution in the different control subspaces for ADT-IMs, where such harmonics are mainly due to the converter and windings non-idealities. For ADT-IPMSMs, the developed harmonics are mainly due to the permanent magnet (PM) non-sinusoidal distribution in the air-gap. Compensating such harmonics is essential towards achieving high-performance operation. Lately, research developed and excelled in achieving a high performance operation of ADT-IPMSMs through realizing, to a high extent, a sinusoidal harmonic-free stator currents. This was accomplished by means of anti-, synchronous proportional-integral-resonant (PIR) controllers [7], multi-resonant controllers [8], and disturbance observers [9]. However, to the best of the authors' knowledge, not much attention has been reported on how to obtain a high fidelity electromechanical model for ADT-IPMSMs in the torque-producing dq frame, which takes into account the fact that IPMSMs are practically *non-linear* machines. Such non-linear model is capable of describing effectively the rated electromechanical torque as well as anticipating the electrical transients.

This paper demonstrates a mathematical model capable of generating both: the fundamental and harmonic elements in the dq frame of ADT-IPMSMs, which are practically *non-linear* machines. The generated electromechanical torque is a function of both the fundamental and harmonic elements. The fundamental dynamics are identified by means of the experimentally identified fundamental flux linkage maps, while the harmonics are generated by means of the experimentally identified harmonic flux linkage parameters through an open circuit test. The cross-coupling between the fundamental dq subspace flux-linkages (i.e. due to saturation) is taken into account. The fundamental flux linkage maps are adopted in designing the dq current controller. The entire experiments and conclusions rely on the stator current measurements and encoder feedback, which is a standard in drive systems, without prior knowledge of the geometric machine design or finite element data. It is also concluded that taking into account the ADT-IPMSM non-linearity increases the expected torque density of the machine and enhances the operation on the Maximum-Torque-per-Ampere (MTPA) current loci [10]–[12]. Using the flux linkage maps, the computed electromechanical torque is compared to the computed torque from the manufacturer parameters and literature, at the same conditions, showing the superiority of the proposed method. A 2.5 kW ADT-IPMSM experimental setup was employed for validation.

II. Asymmetrical dual three phase drive model

A. Dual three phase IPMSM model

For a DTM double-star neutral drive, a generalized Clarke's transformation, also known as vector space decomposition (VSD) [3], is given by

$$\boldsymbol{T}_{\mathrm{VSD}} = \frac{1}{3}\begin{bmatrix} 1 & -\frac{1}{2} & -\frac{1}{2} & \frac{\sqrt{3}}{2} & -\frac{\sqrt{3}}{2} & 0 \\ 0 & \frac{\sqrt{3}}{2} & -\frac{\sqrt{3}}{2} & \frac{1}{2} & \frac{1}{2} & -1 \\ 1 & -\frac{1}{2} & -\frac{1}{2} & -\frac{\sqrt{3}}{2} & \frac{\sqrt{3}}{2} & 0 \\ 0 & -\frac{\sqrt{3}}{2} & \frac{\sqrt{3}}{2} & \frac{1}{2} & \frac{1}{2} & -1 \end{bmatrix}, \quad (1)$$

which decomposes the asymmetrical six-phases quantities $\boldsymbol{f}_{\mathrm{s}}^{a_1\to c_2}$, where $f \in \{u, \psi, i\}$, to two orthogonal planes $\left(f_{\mathrm{s}}^{\alpha\beta},\ \ f_{\mathrm{s}}^{xy}\right) = \boldsymbol{T}_{\mathrm{VSD}}\boldsymbol{f}_{\mathrm{s}}^{a_1\to c_2}$, namely the equivalent $\alpha\beta$ subspace and the xy subspace, which controls the degree of unbalance between the three-phase sets and derating factors during faults [1], [3], [13]. The VSD matrix maps different harmonics to such subspaces, where $\alpha\beta$ plane holds the $12\gamma \pm 1$ harmonics, where $\gamma = \{1, 2, 3, ...\}$, xy is concerned with the $6\Gamma \pm 1$ harmonics, where $\Gamma = \{1, 3, 5, ...\}$. Using the generalized Park's transformation [7]

$$\overline{\boldsymbol{T}}_{\mathrm{p}}(\phi_{\mathrm{e}})^{-1} \ = \ \begin{bmatrix} \boldsymbol{T}_{\mathrm{p}}(\phi_{\mathrm{e}})^{-1} & \boldsymbol{O}_2 \\ \boldsymbol{O}_2 & \boldsymbol{I}_2 \end{bmatrix}, \quad (2)$$

where $\boldsymbol{T}_{\mathrm{p}}(\phi_{\mathrm{e}})^{-1} = \begin{bmatrix} \cos(\phi_{\mathrm{e}}) & -\sin(\phi_{\mathrm{e}}) \\ \sin(\phi_{\mathrm{e}}) & \cos(\phi_{\mathrm{e}}) \end{bmatrix}$, the ADTM-IPMSM dynamic model is

TABLE I. Parameters of the ADT-IPMSM drive.

Parameter	Value
Stator resistance	$R_{\mathrm{s}} = 1.1\,\Omega$
Nominal d-axis inductance*	2 mH
Nominal q-axis inductance*	11.5 mH
Computed d-axis inductance**	6.7 mH
Computed q-axis inductance**	20 mH
Leakage inductance	$L_l = 0.9$ mH
Pole-pair	$n_{\mathrm{p}} = 3$
Inertia	$\Theta = 0.01$ kg·m^2
Viscous friction	$\nu = 0.8 \times 10^{-3}$ N·m·s
Coulomb friction	$m_{\mathrm{c}} = 0.2725$ N·m
Rated stator current	$i_{\mathrm{s,rated}} = 4.2$ A
Rated torque	$m_{\mathrm{e,rated}} = 10.6$ N·m
Rated mechanical speed	2300 RPM
DC-link voltage	$u_{\mathrm{dc}} = 580$ V
Sampling and switching rates	$f_{\mathrm{sw}} = 8$ kHz

* Half the manufacturer's value of the original three-phase machine due to halving the number of turns when carrying-out the rewinding to the dual three-phase machine.
** Computed as shown in [15, Sec. 5.3].

$$\left.\begin{aligned} \overline{\boldsymbol{u}}_{\mathrm{s}}^{dq} &= R_{\mathrm{s}}\,\overline{\boldsymbol{i}}_{\mathrm{s}}^{dq} + \omega_{\mathrm{e}}\,\boldsymbol{J}\overline{\boldsymbol{\psi}}_{\mathrm{s}}^{dq} + \tfrac{\mathrm{d}}{\mathrm{d}t}\overline{\boldsymbol{\psi}}_{\mathrm{s}}^{dq}, \\ \boldsymbol{u}_{\mathrm{s}}^{xy} &= R_{\mathrm{s}}\,\boldsymbol{i}_{\mathrm{s}}^{xy} + L_l\tfrac{\mathrm{d}}{\mathrm{d}t}\boldsymbol{i}_{\mathrm{s}}^{xy}, \\ \tfrac{\mathrm{d}}{\mathrm{d}t}\omega_{\mathrm{e}} &= \tfrac{n_{\mathrm{p}}}{\Theta}\left(m_{\mathrm{e}} - m_{\mathrm{load}} - \nu\,\tfrac{\omega_{\mathrm{e}}}{n_{\mathrm{p}}} - m_{\mathrm{c}}\right), \end{aligned}\right\} \quad (3)$$

where $\boldsymbol{J} := \boldsymbol{T}_{\mathrm{p}}(\pi/2)^{-1}$, $\boldsymbol{i}_{\mathrm{s}}^{xy} = \left(i_{\mathrm{s}}^{x},\ \ i_{\mathrm{s}}^{y}\right)^{\top}$. $\overline{\boldsymbol{f}}_{\mathrm{s}}^{dq} = \left(\overline{f}_{\mathrm{s}}^{d},\ \ \overline{f}_{\mathrm{s}}^{q}\right)^{\top}$, where $f \in \{\psi, u, i\}$, is the total (i.e. fundamental and harmonic elements) flux linkage/voltage/current, respectively, in the dq frame. Note that the dq and xy are decoupled subspaces, thus, the xy plane do not interfere in the torque production mechanism [7], [8], [14]. The ADT-IPMSM parameters are shown in Table I. The model in (3) allows for non-linear flux linkage variation in the dq frame with the corresponding currents. Thus, in this paper, the dq flux linkages are used as *states* instead of currents.

B. dq flux linkage and torque models

The unique difference between different ADTMs is how $\overline{\boldsymbol{\psi}}_{\mathrm{s}}^{dq}$ in (3) is modelled. Unlike the flux linkage models and the assumed constant dq inductances presented in [8], [15], [16], the current-dependency of inductance matrices as well as the harmonic flux linkages are considered in the proposed model [20, Chap. 14]. As explained in Sect. II-A, the dq frame holds the fundamental component, which contributes mainly to the average electromechanical torque and the dq harmonic fluxes, sourced by the PM harmonics, contribute to the oscillating torque. Accordingly, in order to show the total generated electromechanical torque, it is necessary to have a dynamic model capable of modeling both the fundamental and harmonic components. Thus, $\overline{\boldsymbol{\psi}}_{\mathrm{s}}^{dq}$ in (3) can be written as

$$\overline{\boldsymbol{\psi}}_{\mathrm{s}}^{dq} = \boldsymbol{\psi}_{\mathrm{s}}^{dq} + \boldsymbol{\psi}_{\mathrm{s,PM}}^{dq}, \quad (4)$$

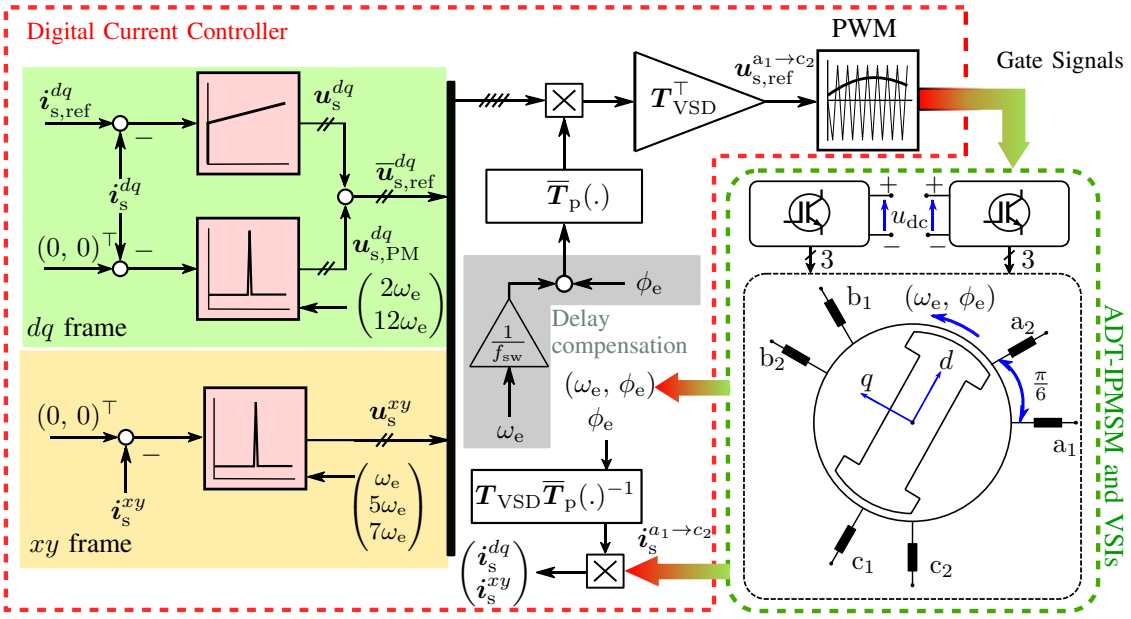

Fig. 1. Proportional-integral and resonant current controllers for the dq and xy frames with the corresponding resonant frequencies for an ADT-IPMSM [8].

where, $\boldsymbol{\psi}_{\mathrm{s}}^{dq}$ is the fundamental flux linkage term, while $\boldsymbol{\psi}_{\mathrm{s,PM}}^{dq}$ is the harmonic term. The same principle is applied to decompose $\overline{\boldsymbol{u}}_{\mathrm{s}}^{dq}$ into fundamental and harmonic components.

As for $\overline{\boldsymbol{i}}_{\mathrm{s}}^{dq}$, the impedance of the dq frame is assumed to be large enough to neglect $\boldsymbol{i}_{\mathrm{s,PM}}^{dq}$ (i.e. $\overline{\boldsymbol{i}}_{\mathrm{s}}^{dq} \approx \boldsymbol{i}_{\mathrm{s}}^{dq}$). With that approximation in mind, the electromechanical torque produced is denoted by

$$\overline{m}_{\mathrm{e}} = 3n_{\mathrm{p}} {\boldsymbol{i}_{\mathrm{s}}^{dq}}^{\top} \boldsymbol{J} \left(\boldsymbol{\psi}_{\mathrm{s}}^{dq} + \boldsymbol{\psi}_{\mathrm{s,PM}}^{dq}\right) = m_{\mathrm{e}} + m_{\mathrm{e,PM}}, \quad (5)$$

where the first term in (5) is the average torque generated by the fundamental component, while the second term represents the oscillatory torque term.

Assuming that non-fundamental components are compensated, as shown later in Sect. III-B, the relation between $\boldsymbol{\psi}_{\mathrm{s}}^{dq}$ and $\boldsymbol{i}_{\mathrm{s}}^{dq}$ is *non-linear* with a cross-coupling between the dq coordinates. This is mathematically modeled as

$$\tfrac{\mathrm{d}}{\mathrm{d}t}\boldsymbol{\psi}_{\mathrm{s}}^{dq} = \boldsymbol{L}_{\mathrm{s}}^{dq}(\boldsymbol{i}_{\mathrm{s}}^{dq}) \tfrac{\mathrm{d}}{\mathrm{d}t}\boldsymbol{i}_{\mathrm{s}}^{dq}, \quad (6)$$

where $\boldsymbol{L}_{\mathrm{s}}^{dq}(\boldsymbol{i}_{\mathrm{s}}^{dq})$ is the *differential* inductance matrix [20, Chap. 14] and is defined as

$$\boldsymbol{L}_{\mathrm{s}}^{dq}(\boldsymbol{i}_{\mathrm{s}}^{dq}) := \begin{bmatrix} \frac{\partial \psi_{\mathrm{s}}^{d}}{\partial i_{\mathrm{s}}^{d}} & \frac{\partial \psi_{\mathrm{s}}^{d}}{\partial i_{\mathrm{s}}^{q}} \\ \frac{\partial \psi_{\mathrm{s}}^{q}}{\partial i_{\mathrm{s}}^{d}} & \frac{\partial \psi_{\mathrm{s}}^{q}}{\partial i_{\mathrm{s}}^{q}} \end{bmatrix} = \begin{bmatrix} L_{\mathrm{s}}^{d} & L_{m}^{dq} \\ L_{m}^{dq} & L_{\mathrm{s}}^{q} \end{bmatrix}. \quad (7)$$

This approach is similar to that shown in [17], which is also known as the flux linkage maps and the corresponding differential inductances identification. The current vector $\boldsymbol{i}_{\mathrm{s}}^{dq}$ is varied to cover the entire operating range of the adopted ADT-IPMSM at a given speed. In the xy frame, the reference currents are set to $\boldsymbol{i}_{\mathrm{s,ref}}^{xy} = (0,\, 0)^{\top}$, as shown in Fig 1. Finally, for the given R_{s} in Table I and a non-zero speed (i.e. $\omega_{\mathrm{e}} \neq 0$) at *steady-state*, the flux linkage vector is obtained by

$$\boldsymbol{\psi}_{\mathrm{s}}^{dq} = \frac{\boldsymbol{J}^{-1}}{\omega_{\mathrm{e}}} \left(\boldsymbol{u}_{\mathrm{s}}^{dq} - R_{\mathrm{s}}\, \boldsymbol{i}_{\mathrm{s}}^{dq}\right). \quad (8)$$

The acquired flux linkages and the corresponding differential inductances are shown in Figs. 2(a)-(b) and Figs. 3(a)-(c), respectively.

Since the dq frame encompasses the rotor 11^{th} and 13^{th} harmonics, applying Park's transformation in (2) maps such harmonics in the dq plane, rotating at $12\omega_{\mathrm{e}}$. The proposed model for $\boldsymbol{\psi}_{\mathrm{s,PM}}^{dq}$ is

$$\boldsymbol{\psi}_{\mathrm{s,PM}}^{dq} = \begin{pmatrix} \psi_{\mathrm{pm}}^{13} \sin(12\omega_{\mathrm{e}}t + \phi_{\mathrm{o}}^{13}) - \psi_{\mathrm{pm}}^{11} \sin(12\omega_{\mathrm{e}}t + \phi_{\mathrm{o}}^{11}) \\ \psi_{\mathrm{pm}}^{13} \cos(12\omega_{\mathrm{e}}t + \phi_{\mathrm{o}}^{13}) + \psi_{\mathrm{pm}}^{11} \cos(12\omega_{\mathrm{e}}t + \phi_{\mathrm{o}}^{11}) \end{pmatrix}, \quad (9)$$

where the constants ψ_{pm}^{11}, ψ_{pm}^{13}, ϕ_{o}^{11}, and ϕ_{o}^{13} are identified through the open circuit test as explained in Sect. IV. Finally the equivalent fundamental and harmonic circuit for the dq frame is shown in Fig. 4.

III. ADT-IPMSM Current Controller

A. PI current controllers and disturbance compensation

Upon computing the flux linkage maps and the corresponding differential inductances, the PI controllers in Fig. 1 are designed according to the magnitude optimum criterion along with updating the PI controller gain and time constant [17]. Accordingly, the proportional V_p and integral time constant T_i of the non-linear PI controllers are defined as

$$\left.\begin{aligned} \begin{pmatrix} V_p^d & V_p^q \end{pmatrix}^{\top} &= \tfrac{f_{\mathrm{sw}}}{2} \begin{pmatrix} \hat{L}_{\mathrm{s}}^{d} & \hat{L}_{\mathrm{s}}^{q} \end{pmatrix}^{\top}, \\ \begin{pmatrix} T_i^d & T_i^q \end{pmatrix}^{\top} &= \tfrac{1}{R_{\mathrm{s}}} \begin{pmatrix} \hat{L}_{\mathrm{s}}^{d} & \hat{L}_{\mathrm{s}}^{q} \end{pmatrix}^{\top}, \end{aligned}\right\} \quad (10)$$

where

$$\begin{pmatrix} \hat{L}_{\mathrm{s}}^{d} & \hat{L}_{\mathrm{s}}^{q} \end{pmatrix}^{\top} = \det\left(\boldsymbol{L}_{\mathrm{s}}^{dq}(\boldsymbol{i}_{\mathrm{s}}^{dq})\right) \begin{pmatrix} \frac{1}{L_{\mathrm{s}}^{q}} & \frac{1}{L_{\mathrm{s}}^{d}} \end{pmatrix}^{\top}. \quad (11)$$

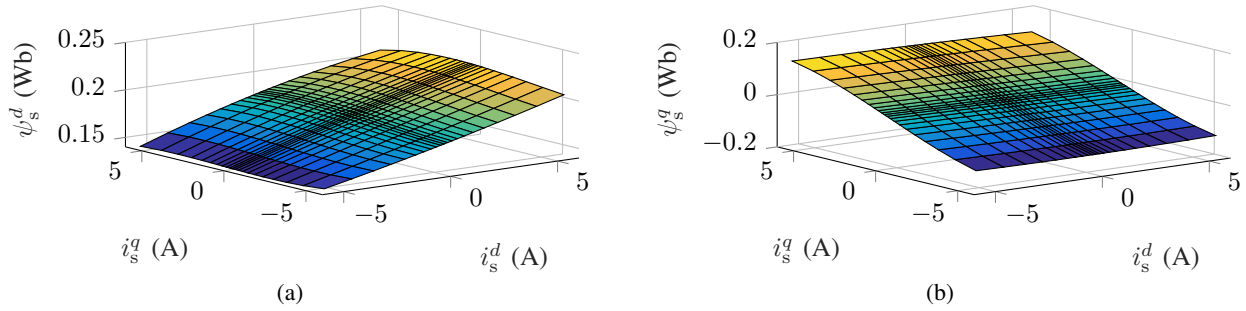

Fig. 2. Measured flux linkage maps of $\boldsymbol{\psi}_{\mathrm{s}}^{dq}$ in (3), showing the variation of (a) ψ_{s}^{d} and ψ_{s}^{q} for $||\boldsymbol{i}_{\mathrm{s}}^{dq}|| \leq i_{\mathrm{s,rated}}$.

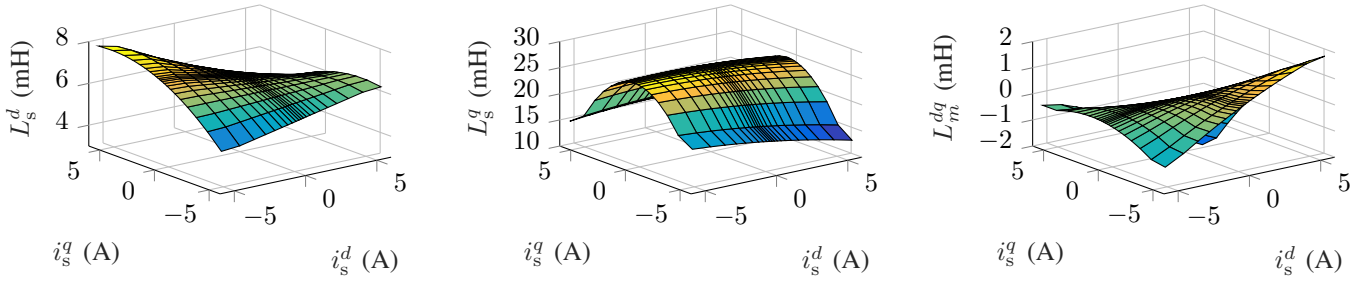

Fig. 3. Measured differential inductances of $\boldsymbol{L}_{\mathrm{s}}^{dq}(\boldsymbol{i}_{\mathrm{s}}^{dq})$ for $||\boldsymbol{i}_{\mathrm{s}}^{dq}|| \leq i_{\mathrm{s,rated}}$ (left to right): (a) L_{s}^{d}, (b) L_{s}^{q}, and (c) L_{m}^{dq}.

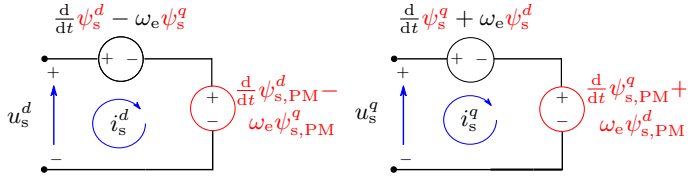

Fig. 4. Proposed equivalent circuits for the dq frame along with highlighting in red the enhanced model elements as explained in Subsect. II-A.

In [17], the disturbance feedforward compensation enhances the tracking speed of the PI controllers. The disturbance voltage $\boldsymbol{u}_{\mathrm{s,dist}}^{dq}$ encompasses the coupling terms between the dq frame coordinates, assuming the machine parameters are identified, which is the case here upon computing $\boldsymbol{\psi}_{\mathrm{s}}^{dq}$ and $\boldsymbol{L}_{\mathrm{s}}^{dq}(\boldsymbol{i}_{\mathrm{s}}^{dq})$. As proven in [17], $\boldsymbol{u}_{\mathrm{s,dist}}^{dq}$ is computed by

$$\begin{aligned}\boldsymbol{u}_{\mathrm{s,dist}}^{dq} \;=\; -L_m^{dq}\begin{bmatrix} 0 & \frac{1}{\hat{L}_{\mathrm{s}}^{q}} \\ \frac{1}{\hat{L}_{\mathrm{s}}^{d}} & 0 \end{bmatrix}\left(\boldsymbol{u}_{\mathrm{s}}^{dq} - R_{\mathrm{s}}\,\boldsymbol{i}_{\mathrm{s}}^{dq} - \right. \\ \left. \omega_{\mathrm{e}}\,\boldsymbol{J}\boldsymbol{\psi}_{\mathrm{s}}^{dq}\right) - \omega_{\mathrm{e}}\,\boldsymbol{J}\boldsymbol{\psi}_{\mathrm{s}}^{dq}.\end{aligned} \tag{12}$$

B. Resonant (R) controllers

As illustrated in Sect. II-A, the presence of harmonic flux linkage elements in the dq and xy frames invokes the presence of harmonic currents within such frames. Compensating such current harmonics is inevitable to guarantee high quality performance for the employed ADT-IPMSM drive. This could be achieved either by adopting multi-synchronous frames in both the dq and xy frames [7] or by invoking multi-resonant controllers for the shown model in (3) [8]. The latter method is the one adopted in this paper. Since the amplitude of harmonic currents are speed dependent, meaning they are boosted/curtailed with the increase/decrease of ω_{e}, the resonant (R) controllers are expected to be speed-dependent tuned. The R-controllers are discretized using the impulse-invariant method to ensure precise lock on the desired resonant frequency ω_{R} as well as stable operation [8], [18]. The time constant of such R-controllers T_{R} is carried out similar to the method shown in [8] which leads to

$$\begin{pmatrix} T_{\mathrm{R}}^{d} & T_{\mathrm{R}}^{q} & T_{\mathrm{R}}^{xy} \end{pmatrix} = \frac{100}{R_{\mathrm{s}}\omega_{\mathrm{e}}}\begin{pmatrix} \hat{L}_{\mathrm{s}}^{d} & \hat{L}_{\mathrm{s}}^{q} & L_l \end{pmatrix}, \tag{13}$$

where $(T_{\mathrm{R}}^{d},\, T_{\mathrm{R}}^{q})$ are adapted online with L_{s}^{d} and L_{s}^{q}, respectively. The tuned resonant frequencies of the R-controllers in the dq and xy frames are ω_{R}^{dq} and ω_{R}^{xy}, respectively. As seen in Fig. 1, there are two pairs of R-controllers in the dq frame where $\omega_{\mathrm{R}}^{dq} = (2\omega_{\mathrm{e}},\, 12\omega_{\mathrm{e}})$, while three pairs of R-controllers in the xy frame, tuned at $\omega_{\mathrm{R}}^{xy} = (\omega_{\mathrm{e}},\, 5\omega_{\mathrm{e}},\, 7\omega_{\mathrm{e}})$.

IV. Evaluation Results

A. Experimental environment

This section evaluates the outcomes of the proposed model on a practical setup, shown in Fig. 5, having the same parameters as indicated in Table I. The test bench in Fig. 5 consists of an ADT-IPMSM tied to a standard three-phase induction machine acting as the prime mover. With the aid of Matlab/Simulink, the control algorithm is implemented on dSPACE DS1007. The PWM signals are sent to the VSIs via the DS5101 PWM card, where the triggering signals are manually programmed to ensure precise timings and sampling

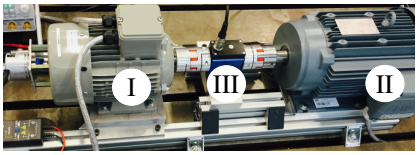

Fig. 5. Test bench: (I) ADT-IPMSM, (II) induction machine (i.e. prime mover) and (III) torque sensor.

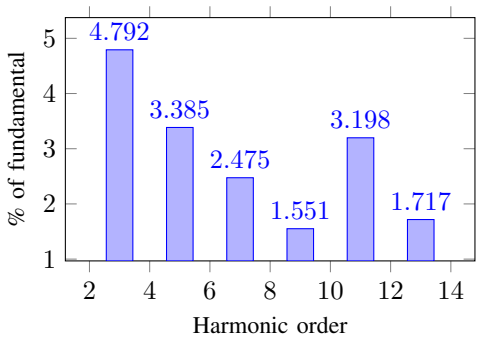

Fig. 6. Back-*e.m.f* harmonic content of the ADT-IPMSM at 1000 RPM.

TABLE II. FFT of the rotor flux linkage at 1000 RPM.

Order	Magnitude (Wb)	Phase (rad)
1	180×10^{-3}	0
11	$\psi_{\mathrm{pm}}^{11} = 5.1 \times 10^{-3}$	$\phi_{\mathrm{o}}^{11} = 3.5168$
13	$\psi_{\mathrm{pm}}^{13} = 2.4 \times 10^{-3}$	$\phi_{\mathrm{o}}^{13} = 0.4224$

instants. The A/D DS2004 board is triggered by the DS5101 board to carry-out the measurements in the middle of the switching period. The real-time control structure is similar to the indicated block diagram in Fig. 1. The discrete-time delay in the position measurement is compensated when applying the Park transformation (i.e. $\overline{\boldsymbol{T}}_{\mathrm{p}}(\phi_{\mathrm{e}} + \omega_{\mathrm{e}}/f_{\mathrm{sw}})$), as highlighted in Fig. 1 [19]. To identify the constants in (9), the ADT-IPMSM is open circuited and rotated at a constant speed of 1000 RPM. The back-*e.m.f* was measured using an oscilloscope and analyzed using Fast Fourier Transform (FFT) shown in Fig. 6, from which the flux-linkage harmonic content was estimated as shown in Table II. Moreover, the electromechanical torque is computed on dSPACE three times using the flux linkage maps in (5), obtained parameters in [15, Sec. 5.3], and the manufacturer parameters. The computed electromechanical torques are compared against the practically developed electromechanical torque, after compensating the torque losses (i.e. due to coulomb and viscous friction in (3) and using the parameters in Table I) [20, Sec. 11.1.5].

B. Transient and steady-state responses

The electromechanical transients are directly affected by the dq frame dynamics. In order to evaluate the transient response for the proposed dq controllers in Sect. III, the reference dq currents (i.e. $\boldsymbol{i}_{\mathrm{s,ref}}^{dq}$) are varied within a 0.5 s window, while monitoring the current transients during current references steps at 800 RPM. Fig. 7 illustrates the aforementioned current

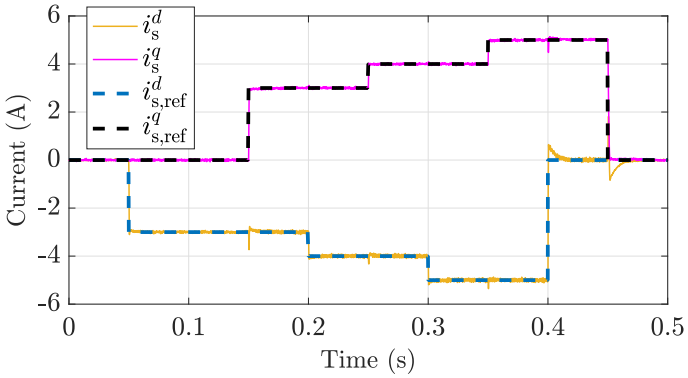

Fig. 7. Experimental transient response for the proposed current controller in the dq frame as shown in Sect. III.

references with the corresponding $\boldsymbol{i}_{\mathrm{s}}^{dq}$. From Fig. 7, complete decoupling between the dq coordinates (i.e. disturbance compensation) could not be achieved; due to the presence of the R-controllers which exhibits some transients during changes in $\boldsymbol{i}_{\mathrm{s,ref}}^{dq}$. The settling times for a 2% error criteria were 0.62 ms and 1.2 ms for the dq coordinates, respectively. The settling times were larger when the reference currents were regulated to zero, which lead to dq settling times of 6.8 ms and 8 ms, respectively. The reported results are considered still acceptable.

For the steady-state evaluation, the harmonic spectrum of the stator currents was analyzed through FFT upon applying a given current reference of $\boldsymbol{i}_{\mathrm{s,ref}}^{dq} = (-3.78, -3.78)$ A. The resulted six phase currents are shown in Fig. 8(a). The FFT analysis shown in Fig. 8(b) indicate that the proposed controller is able to suppress the harmonic currents according to the indicated resonant frequencies shown in Fig. 1. A total harmonic distortion (THD) of 0.98% is reported. Furthermore, the measured electromechanical torque is compared with the computed torques leading to the results shown in Fig. 9, indicating the effectiveness of the proposed electromechanical torque model using the non-linear flux linkage maps in (5).

C. Torque maps and MTPA criteria

The proposed electromechanical model using the flux maps in (5) is evaluated in the entire dq space compared to the linear flux linkages assumptions provided by the manufacturer and proposed method in [15, Sec. 5.3]. This is done by forcing $\boldsymbol{i}_{\mathrm{s,ref}}^{dq}$ through the entire dq space resulting in a surface plot defined as *torque maps*. By plotting the difference between the measured torque and computed torques, the outcomes are shown in Fig. 10, indicating that the proposed method produces the minimal error compared to the linear flux linkage method. It should be noted that the error between the proposed method and the measured electromechanical torque in Fig. 10(c) is not perfectly zero; since the acquired flux linkage maps in Fig. 2(a)-(b) had undergone some off-line smoothing leading to numerical errors. Furthermore, compensating the effect of torque losses is not perfect over the entire speed range. Nevertheless, the errors in Fig. 10(a)-(b) tend to increase and

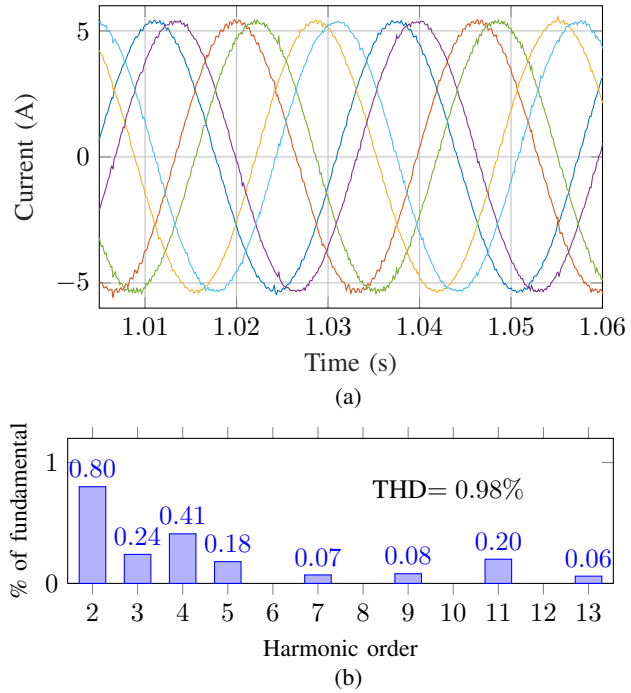

Fig. 8. (a) Stator currents and the corresponding (b) FFT at steady-state for $\boldsymbol{i}_{\mathrm{s,ref}}^{dq} = (-3.78,\ -3.78)^{\top}$ A and $\boldsymbol{i}_{\mathrm{s,ref}}^{xy} = (0,\ 0)^{\top}$ A.

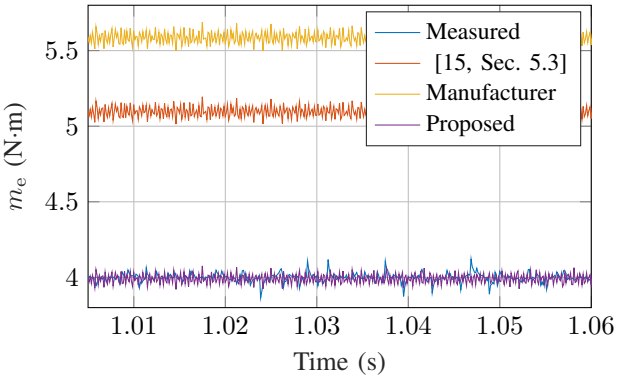

Fig. 9. Comparison between the electromechanical torques computed using the parameters acquired by different methods and the measured one.

vary as the operating point is not in the vicinity of the origin point; since the effect of saturation and coupling between the dq coordinates starts to prevail.

On the other hand, it is possible to use torque map using the non-linear flux linkage to obtain the MTPA loci, which are obtained by calculating the minimum current magnitude $||\boldsymbol{i}_{\mathrm{s}}^{dq}||$ for a given measured torque. The new MTPA loci is shown in Fig. 11. It is clear that using non-linear flux linkage maps results in different MTPA loci compared to computing such loci with constant parameters. In other words, the proposed method leads to an optimum MTPA current reference generation compared to the other methods (i.e. reduced copper losses) [10]–[12]. By defining the stator copper losses as $P_{\mathrm{Cu}} := 3\,||\boldsymbol{i}_{\mathrm{s}}^{dq}||^2\,R_{\mathrm{s}}$ (assuming $\boldsymbol{i}_{\mathrm{s}}^{xy}$ is regulated to *zero*), Fig. 12 shows the percentage errors between the stator copper losses $\Delta P_{\mathrm{Cu}}\%$ produced by the MTPA loci, obtained by the manufacturer's and [15, Sec. 5.3] parameters, and the non-linear flux linkage maps. Thus, the effectiveness of the proposed method is verified.

V. Conclusion

In this paper, an enhanced electromechanical model was presented for ADT-IPMSMs, relying on estimating the non-linear flux linkages, from which the differential inductances are identified, taking into account the cross-coupling between the dq coordinates and saturation. The dq harmonics, due to the PM flux harmonics, are also identified. The PI and R-controllers were tuned and operating-point adaptive depending on the obtained non-linear flux linkages. The non-linear flux linkages affects both the generated electromechanical torque and the MTPA current loci, which have been evaluated against assuming linear flux linkages as given by the manufacturer and estimated by recent literature. Thus, the motivation of employing such non-linear flux linkage maps, in terms of modeling and control has been verified. The theoretical findings were corroborated with a 2.5 kW ADT-IPMSM setup for the sake of validation.

Acknowledgment

This work is supported by the project AWESCO (H2020-ITN-642682) funded by the European Union's Horizon 2020 research and innovation program under the Marie Sklodowska-Curie grant agreement No. 642682.

References

[1] I. Gonzalez-Prieto, M. J. Duran, H. S. Che, E. Levi, M. Bermúdez, and F. Barrero, "Fault-tolerant operation of six-phase energy conversion systems with parallel machine-side converters," *IEEE Trans. on Power Electron.*, vol. 31, pp. 3068–3079, Apr. 2016.

[2] D. Hadiouche, H. Razik, and A. Rezzoug, "On the modeling and design of dual-stator windings to minimize circulating harmonic currents for vsi fed ac machines," *IEEE Trans. on Ind. Appl.*, vol. 40, pp. 506–515, Mar. 2004.

[3] W. N. W. A. Munim, M. Duran, H. S. Che, M. Bermudez, I. Gonzalez-Prieto, and N. A. Rahim, "A unified analysis of the fault tolerance capability in six-phase induction motor drive," *IEEE Trans. on Power Electron.*, vol. 32, no. 10, pp. 7824–7836, 2016.

[4] D. Dujic, E. Levi, and M. Jones, "DC bus utilisation in multiphase vsi supplied drives with a composite stator phase number," in *2010 IEEE Int. Conf. on Ind. Technology*, pp. 1495–1500, Mar. 2010.

[5] S. Hu, Z. Liang, W. Zhang, and X. He, "Research on the integration of hybrid energy storage system and dual three-phase pmsm drive in ev," *IEEE Trans. on Ind. Electron.*, (early-access), 2017 (doi:10.1109/TIE.2017.2752141).

[6] Y. Zhao and T. A. Lipo, "Space vector pwm control of dual three-phase induction machine using vector space decomposition," *IEEE Trans. on Ind. Appl.*, vol. 31, pp. 1100–1109, Sep. 1995.

[7] Y. Hu, Z. Q. Zhu, and K. Liu, "Current control for dual three-phase permanent magnet synchronous motors accounting for current unbalance and harmonics," *IEEE Journal of Emerging and Selected Topics in Power Electron.*, vol. 2, pp. 272–284, Jun. 2014.

[8] A. G. Yepes, J. Doval-Gandoy, F. Baneira, D. Perez-Estevez, and O. Lopez, "Current harmonic compensation for n-phase machines with asymmetrical winding arrangement and different neutral configurations," *IEEE Trans. on Ind. Appl.*, vol. 53, no. 6, pp. 5426–5439, 2017.

[9] J. Karttunen, S. Kallio, P. Peltoniemi, and P. Silventoinen, "Current harmonic compensation in dual three-phase pmsms using a disturbance observer," *IEEE Trans. on Ind. Electron.*, vol. 63, pp. 583–594, Jan. 2016.

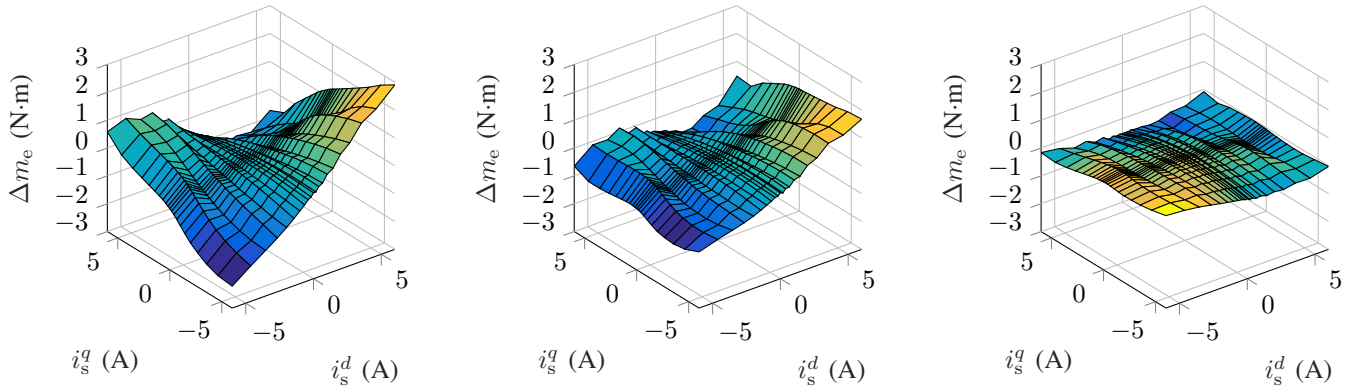

Fig. 10. Error between the measured electromechanical torque and the computed one using the parameters provided by (a) the manufacturer, (b) [15, Sec. 5.3], and (c) the non-linear flux linkage maps.

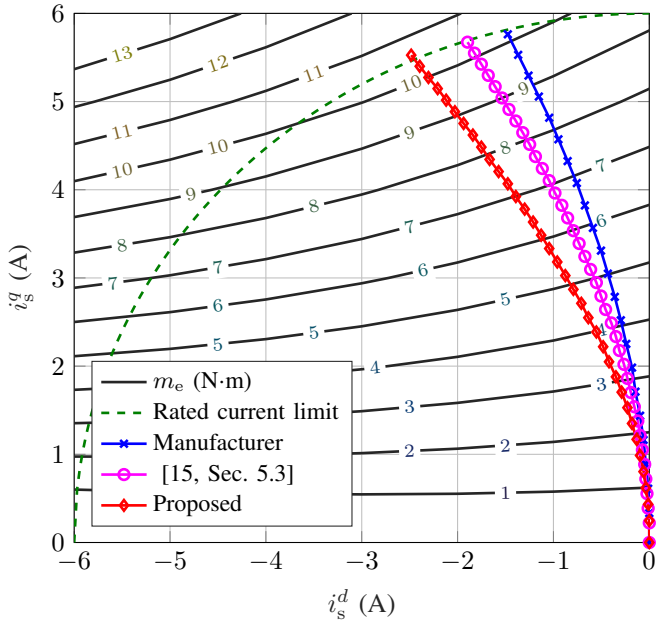

Fig. 11. MTPA current loci for the different torque computation methods and their intersection with the measured torque parabolas.

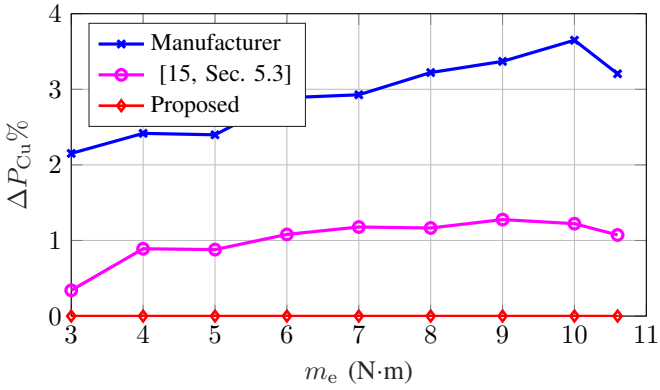

Fig. 12. Comparison of $\Delta P_{\mathrm{Cu}}\%$ computed with the parameters of the different methods with respect to the losses computed when adopting the non-linear flux linkage maps.

[10] R. Ni, D. Xu, G. Wang, L. Ding, G. Zhang, and L. Qu, "Maximum efficiency per ampere control of permanent-magnet synchronous machines," *IEEE Trans. on Ind. Electron.*, vol. 62, pp. 2135–2143, Apr. 2015.

[11] H. Eldeeb, C. M. Hackl, and J. Kullick, "Efficient operation of anisotropic synchronous machines for wind energy systems," *Journal of Physics: Conf. Series*, vol. 753, no. 11, p. 112009, 2016.

[12] H. Eldeeb, C. M. Hackl, L. Horlbeck, and J. Kullick, "A unified theory for optimal feedforward torque control of anisotropic synchronous machines," *Int. Journal of Control*, (open access), pp. 1–30, 2017 (doi:10.1080/00207179.2017.1338359).

[13] W. Wang, J. Zhang, M. Cheng, and S. Li, "Fault-tolerant control of dual three-phase permanent-magnet synchronous machine drives under open-phase faults," *IEEE Trans. on Power Electron.*, vol. 32, pp. 2052–2063, Mar. 2017.

[14] H. S. Che, E. Levi, M. Jones, W. P. Hew, and N. A. Rahim, "Current control methods for an asymmetrical six-phase induction motor drive," *IEEE Trans. on Power Electron.*, vol. 29, pp. 407–417, Jan. 2014.

[15] S. Kallio, J. Karttunen, P. Peltoniemi, P. Silventoinen, and O. Pyrhonen, "Determination of the inductance parameters for the decoupled d-q model of double-star permanent magnet synchronous machines," *IET Electric Power Appl.*, vol. 8, pp. 39–49, Feb. 2014.

[16] S. Kallio, M. Andriollo, A. Tortella, and J. Karttunen, "Decoupled d-q model of double-star interior-permanent-magnet synchronous machines," *IEEE Trans. on Ind. Electron.*, vol. 60, pp. 2486–2494, Jun. 2013.

[17] C. M. Hackl, M. J. Kamper, J. Kullick, and J. Mitchell, "Current control of reluctance synchronous machines with online adjustment of the controller parameters," in *in Proc. of the 2016 IEEE Int. Symp. on Ind. Electron. (ISIE 2016)*, (Santa Clara, CA, USA), pp. 156–160, 2016.

[18] H. Eldeeb, A. Massoud, A. S. Abdel-Khalik, and S. Ahmed, "A sensorless kalman filter-based active damping technique for grid-tied vsi with lcl filter," *Int. Journal of Electrical Power & Energy Systems*, vol. 93, pp. 146 – 155, 2017.

[19] Y. A.-R. I. Mohamed and E. F. El-Saadany, "An improved deadbeat current control scheme with a novel adaptive self-tuning load model for a three-phase pwm voltage-source inverter," *IEEE Trans. on Ind. Electron.*, vol. 54, pp. 747–759, Apr. 2007.

[20] C. M. Hackl, *Non-identifier based adaptive control in mechatronics: Theory and Application*. Lecture Notes in Control and Information Sciences, Berlin: Springer-Verlag, 2017.